Applied Physics Letters

Magnetic damping in poly-crystalline $Co_{25}Fe_{75}$: Ferromagnetic resonance vs. spin wave propagation experiments

Cite as: Appl. Phys. Lett. **111**, 132406 (2017); https://doi.org/10.1063/1.4994137
Submitted: 04 July 2017 • Accepted: 02 September 2017 • Published Online: 27 September 2017

H. S. Körner, M. A. W. Schoen, T. Mayer, et al.

Magnetic damping in poly-crystalline $Co_{25}Fe_{75}$: Ferromagnetic resonance vs. spin wave propagation experiments

H. S. Körner, M. A. W. Schoen, T. Mayer, M. M. Decker, J. Stigloher, T. Weindler, T. N. G. Meier, M. Kronseder, and C. H. Back[a)]
Institute of Experimental and Applied Physics, University of Regensburg, D-93040 Regensburg, Germany

(Received 4 July 2017; accepted 2 September 2017; published online 27 September 2017)

We report on the investigation of the magnetic damping of a 10 nm thin, poly-crystalline $Co_{25}Fe_{75}$ film grown by molecular beam epitaxy. Ferromagnetic resonance (FMR) measurements reveal a low intrinsic magnetic damping $\alpha_{int}^{FMR} = (1.5 \pm 0.1) \times 10^{-3}$. In contrast, in patterned micrometer wide stripes, spin wave (SW) propagation experiments performed by time resolved scanning magneto-optical Kerr microscopy yield attenuation lengths on the order of 5–8 μm. From this quantity, we deduce an effective magnetic SW damping $\alpha_{eff}^{SW,exp} = (3.9 \pm 0.3) \times 10^{-3}$. For the system studied, this significant difference between both damping parameters is attributed to the non-negligible extrinsic contributions (local inhomogeneities and two-magnon scattering) to the magnetic losses which manifest themselves as a distinct inhomogeneous FMR linewidth broadening. This explanation is supported by micromagnetic simulations. Our findings prove that poly-crystalline $Co_{25}Fe_{75}$ represents a promising binary 3*d* transition metal alloy to be employed in magnonic devices with much longer SW attenuation lengths compared to other metallic systems. *Published by AIP Publishing*. [http://dx.doi.org/10.1063/1.4994137]

Further advances in the field of magnonics,[1] where spin waves (SW) will be utilized as information carriers, essentially depend on magnetic films in which SWs can propagate over large distances. The corresponding figure of merit is the attenuation length L_{att} being defined as the distance over which the SW amplitude decays to a factor of $1/e$. It strongly depends on the magnetic parameters of the film (saturation magnetization M_S, magneto-crystalline anisotropies, and thickness) and on the magnetization precession losses.[2,3] The latter enter the effective magnetic damping α_{eff} which scales with $1/L_{att}$. Hence, research in the field of magnonics focuses on magnetic materials with low damping. From this perspective, within the last decade, various different materials have been thoroughly investigated.

The ferrimagnetic insulator Yttrium Iron Garnet (YIG) exhibits extremely low damping parameters (on the order of 10^{-5}–10^{-4}),[4,5] but its low M_S (about 0.2 T) results in relatively low group velocities.[6] Moreover, it requires delicate growth techniques, and its integration into micrometer scale spintronic elements remains challenging. Ferromagnetic metal films are considered as promising alternatives. Here, the drawback of a much larger magnetic damping (on the order of $2–8 \times 10^{-3}$) is compensated by a larger M_S (on the order of 1–2 T) and by an easier deposition and integration into spintronic elements. So far, various metals have been explored, e.g., the ferromagnetic metals Permalloy ($Ni_{80}Fe_{20}$, $\alpha \approx 6–8 \times 10^{-3}$, $\mu_0 M_S \approx 1$ T)[7–9] and Fe ($\alpha \approx 2 \times 10^{-3}$, $\mu_0 M_S \approx 2.2$ T),[10] half-metallic Heusler alloys,[11,12] and CoFeB alloys[13] where the fabrication of the latter two with low damping values still remains a delicate issue. Just recently, a very low magnetic damping was theoretically predicted[14] and experimentally verified[15] for the binary 3*d* transition metal alloy Co_xFe_{1-x}, revealing pure intrinsic damping parameters as low as 5×10^{-4} for $Co_{25}Fe_{75}$ (CoFe). In combination with its large M_S (about 2.4 T at room temperature) and its relatively easy deposition, CoFe offers several benefits to become a very promising ferromagnetic metal to be used for magnonic devices.

In this Letter, we study the magnetic damping of a 10 nm thin, poly-crystalline CoFe full film grown by molecular beam epitaxy (MBE). The full film characterization and the determination of the intrinsic magnetic damping are performed by in-plane (IP) ferromagnetic resonance (FMR) measurements. We compare it with the effective magnetic damping deduced from the investigation of the attenuation length of Damon-Eshbach (DE) SWs[16] propagating in micrometer wide stripes patterned from the same CoFe full film. SWs are detected by time resolved scanning magneto-optical Kerr (TRMOKE) microscopy. For the system investigated, we find a distinct difference between the intrinsic and the effective magnetic SW damping parameter which is ascribed to the extrinsic contributions to the magnetic losses arising from local inhomogeneities and two-magnon scattering.[17,18] This explanation is supported by micromagnetic simulations.

A full film sample is grown by MBE on a GaAs(001) substrate which is degassed at 250 °C prior to the co-deposition from Co and Fe sources of a 10 nm thin $Co_{25}Fe_{75}$ layer on a 5 nm thin MgO seed layer. Finally, a MgO (5 nm)/Al_2O_3(7 nm) capping is added to prevent oxidation. The composition of the CoFe layer is verified by X-ray photoelectron spectroscopy with an error of less than 3%. Superconducting quantum interference device measurements at $T = 290$ K reveal $\mu_0 M_S = (2.4 \pm 0.1)$ T which is in good agreement with the literature values.[15] Then, the film is characterized by waveguide-based FMR performed in the IP geometry utilizing a Schottky diode detector and lock-in amplification of the field-modulated signal. Frequencies up to 40 GHz and fields up to 2 T are applied. The FMR data are fitted by the method described in Ref. 19. The extracted

a)Electronic mail: christian.back@physik.uni-regensburg.de

resonance field H_{res} and linewidth ΔH (full width at half maximum) data are shown in Figs. 1(a) and 1(b), respectively. From the Kittel fits of the frequency dependence of H_{res}, we deduce a gyromagnetic ratio γ of 185 rad/(Ts) and an effective magnetization $\mu_0 M_{eff} = (\mu_0 M_S - \mu_0 H_u^{\perp}) = (1.91 \pm 0.02)$ T, where $\mu_0 H_u^{\perp} = (0.49 \pm 0.10)$ T is the strength of the uniaxial perpendicular magnetic anisotropy field. Moreover, we find that the sample is almost magnetically isotropic exhibiting only a small IP uniaxial anisotropy field of $\mu_0 H_u^{IP} = (1.7 \pm 0.2)$ mT which is oriented along the (110) direction of the GaAs substrate as shown in the IP angular dependence of H_{res} in Fig. 1(a). In contrast to the four-fold symmetry characteristic of a crystalline *bcc* system, this uniaxial IP anisotropy is an indicator for the poly-crystalline growth of the CoFe layer being induced by the poly-crystalline or amorphous growth of the MgO seed layer on the native oxide layer on top of the GaAs(001) substrate which was not removed prior to deposition. Similarly, ΔH does not display any dependence on the IP field angle within the error bars as indicated by the red circle in Fig. 1(b). Furthermore, the frequency dependence of ΔH is measured along both the easy and hard axes as shown in Fig. 1(c). The standard procedure to deduce both the intrinsic Gilbert damping parameter α_{int} and the extrinsic contributions to the magnetic damping is to fit these data to $\Delta H(\omega) = (2\alpha_{int}\omega)/(\mu_0\gamma) + \Delta H(\omega = 0)$.[17,18] We obtain $\alpha_{int}^{FMR} = (1.5 \pm 0.1) \times 10^{-3}$ and $\mu_0 \Delta H(\omega = 0) = (2.0 \pm 0.1)$ mT (mean values). Here, the contribution arising from radiative damping, inherently present when performing waveguide-based FMR,[20] is already subtracted. Neither quantity reveals any discernable angular dependence within the error bars. Our α_{int}^{FMR} value is about three times larger than the one reported by Schoen *et al.*[15] in the case of sputtered $Co_{25}Fe_{75}$.

From the full film, 500 μm long and 1.15 μm wide stripes are patterned by electron beam lithography (EBL) and subsequent chemically assisted Ar^+ ion beam etching with their long axis being oriented perpendicular to the easy axis of the uniaxial IP anisotropy. Then, an additional 80 nm thick insulating Al_2O_3 layer is grown by atomic layer deposition to ensure that the CoFe stripes are electrically decoupled from the microwave antennas in the shape of short coplanar waveguides which are fabricated on top by EBL, thermal evaporation of Cr(10 nm)/Au(60 nm) and liftoff as shown in Fig. 2(a).

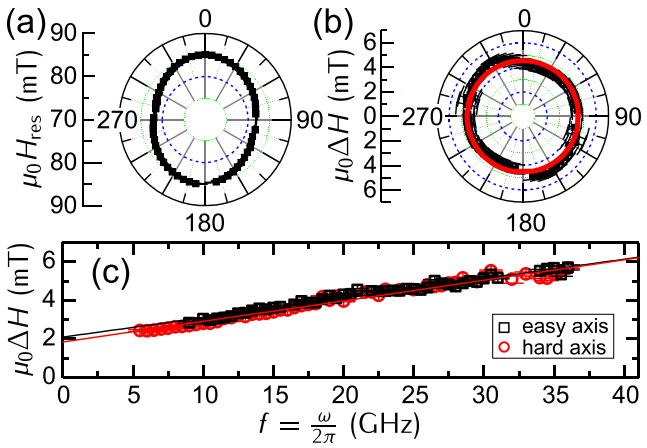

FIG. 1. Full film FMR characterization. (a) and (b) display the angular dependence of the IP resonance field H_{res} and the corresponding linewidth ΔH measured at 12 GHz, respectively. The red circle in (b) visualizes the isotropy of the IP linewidth. (c) Frequency dependence of the IP linewidth extracted from measurements performed with the external magnetic field applied both along the hard axis [i.e., along 0° in (a)] and along the easy axis [i.e., along 90° in (a)]. Solid lines represent the linear fits to the data.

In the CoFe stripes, SW propagation experiments are performed in the DE geometry, i.e., as illustrated in Fig. 2(a), SWs with wave number k are excited by the microwave antenna and propagate along the x direction on either side of the antenna, while the external magnetic bias field H_0 is applied along the z direction. SW dynamics in the stripes is accessed magneto-optically by TRMOKE performed in the polar geometry, i.e., with sensitivity to the dynamic out-of-plane component of the propagating DE SWs, with a spatial resolution of about 250 nm. Details about the setup can be found in Ref. 9. The setup is operated in two modes providing complementary information. In the first mode, for a fixed excitation frequency f, the laser spot is kept at a fixed position on the stripe some micrometer away from the edges of the antenna, while the magnitude of H_0 is swept, enabling us to record SW resonance spectra. From these spectra, we extract the field ranges which are appropriate for the optical detection of propagating SWs at fixed f. Here, we observe SW resonances in the range of 10 to 18 GHz for bias fields ranging from 30 mT up to 180 mT (see supplementary material). Thus, the images and results shown and discussed below are recorded at frequencies around 13.92 GHz at bias fields ranging from 75 to 100 mT. In the second mode, for fixed f and fixed H_0, the sample is scanned in the xz plane, enabling imaging of the propagating DE SWs on either side of the antenna. An example Kerr image is shown in the top panel of Fig. 2(b). In order to exclude the Oersted field of the

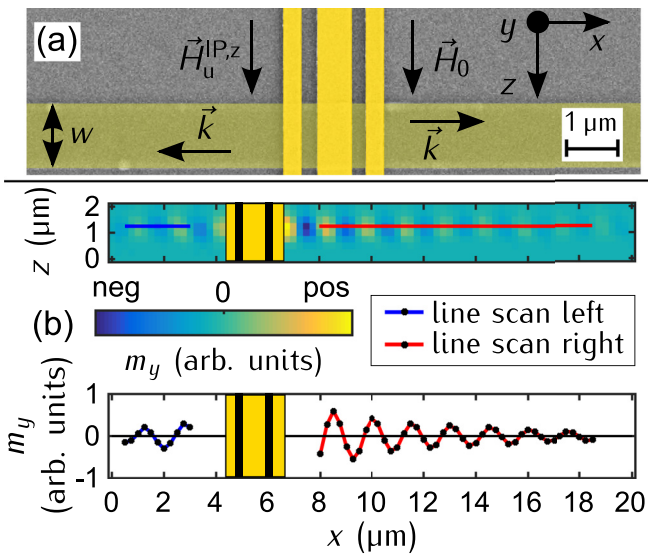

FIG. 2. (a) Scanning electron microscopy image of a section of the patterned stripe sample. The experiment is performed in the DE geometry. In the CoFe stripe (width $w = 1.15$ μm), SWs with wavevector $\vec{k}$ excited by the microwave antenna (yellow) propagate along the x direction on either side of the antenna, while the external magnetic bias field $\vec{H}_0$ is applied along the z direction. The easy axis of the uniaxial IP anisotropy field $\vec{H}_u^{IP,z}$ points along the z direction. (b) (Top panel) Example Kerr image recorded at 13.92 GHz and −90 mT, showing SWs propagating on either side of the antenna and (bottom panel) corresponding line scans extracted along the red and blue lines in the top panel.

microwave antenna, from these images, we extract one-dimensional line scans some micrometer away from the edges of the antenna on either side as depicted in the bottom part of Fig. 2(b). Due to the amplitude non-reciprocity inherently present when exciting DE SWs by a microwave antenna,[21] we focus on the side of the antenna where the Kerr signal is larger for a fixed bias field direction. The line scans are fitted to an exponentially decaying sine function to determine k and L_{att} (see supplementary material). Neglecting the small IP anisotropy, the latter one is given by[2,9]

$$L_{\mathrm{att}} = \frac{2v_{\mathrm{g}}}{\alpha_{\mathrm{eff}}^{\mathrm{SW}}\gamma\mu_0\left(2[H_0 - NM_{\mathrm{S}}] + M_{\mathrm{S}} - H_{\mathrm{u}}^{\perp}\right)}, \qquad (1)$$

where v_{g}, $\alpha_{\mathrm{eff}}^{\mathrm{SW}}$, and N are the group velocity, the effective magnetic SW damping parameter, and the demagnetizing factor along the z direction.[22] We note that due to the finite width w of the stripes, the demagnetizing field and hence the internal magnetic IP field are strongly inhomogeneous across w. However, as a proper derivation of an expression for the demagnetizing field is quite cumbersome,[23] the simplest way to take this effect into account is by adding the term $-NM_{\mathrm{S}}$ which corresponds to the demagnetizing field averaged across w. Since all quantities in Eq. (1) can be obtained experimentally, the value of $\alpha_{\mathrm{eff}}^{\mathrm{SW}}$ can be extracted from the measured values of L_{att} in SW propagation experiments and be subsequently compared to the previously obtained result for $\alpha_{\mathrm{int}}^{\mathrm{FMR}}$.

The evaluation of Kerr images recorded for different combinations of f and H_0 reveals $k(H_0, f)$ and L_{att} (H_0, f) as displayed in Figs. 3(a) and 3(b), respectively. As expected, for fixed f, k decreases linearly with the increasing bias field. The values of L_{att} scatter with average values in the range of 5 to 8 μm. Since the group velocity is given by $v_{\mathrm{g}} = 2\pi\partial f/\partial k$ and $k(f, H_0)$ is recorded for frequencies 240 MHz above and below $f = 13.92$ GHz, it is extracted from linear fits to $f(k)$ for fixed H_0. In the field range studied, we obtain values between 3.8 and 4.5 km/s which are more than twice as large than those for Permalloy[9] and comparable to bulk Fe.[10] Finally, we substitute all the experimentally determined values into Eq. (1) to obtain $\alpha_{\mathrm{eff}}^{\mathrm{SW}}$. Here, we use $N = 0.0172$ being calculated using the analytical expression given in Ref. 22. As shown in Fig. 3(c), we find $\alpha_{\mathrm{eff}}^{\mathrm{SW,exp}} = (3.9 \pm 0.3) \times 10^{-3}$ as the mean value when averaging over the whole studied field range. $\alpha_{\mathrm{eff}}^{\mathrm{SW,exp}}$ is about 2.5 times larger than $\alpha_{\mathrm{int}}^{\mathrm{FMR}}$, thus presenting a distinct difference. Its origin is unveiled in the following by micromagnetic simulations using MuMax3.[24]

Changes in the CoFe quality as well as changes in M_{eff} due to increased temperatures (up to 150 °C) during the fabrication of the stripe samples can be excluded beforehand to result in a significant enhancement of the magnetic damping since FMR measurements on the full film being annealed for several hours reveal no discernable changes for temperatures below 200 °C. This finding does not exclude for instance inhomogeneities inherently present in the CoFe layer after growth as another possible source for an increased magnetic damping which the propagating SWs are subjected to.

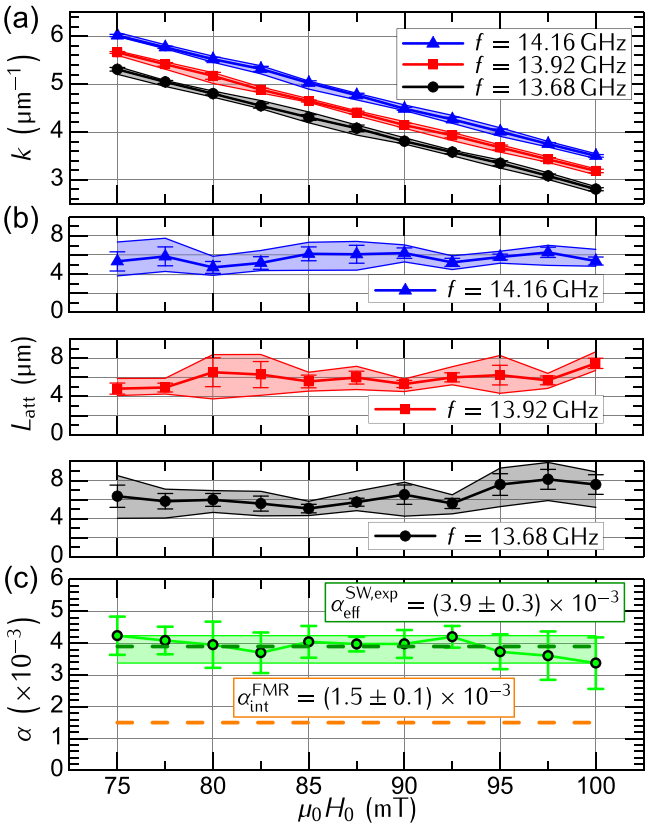

FIG. 3. Field dependence of k (a) and L_{att} (b) for different f values, respectively. (c) Comparison of the damping parameter determined from FMR measurements on CoFe full films with the one obtained from the SW propagation experiments in stripes. Symbols denote mean values, and error bars denote the corresponding standard deviation. Color-shaded areas indicate the range of values of the different quantities (between minimum and maximum), while dashed lines indicate the average values.

The propagation of DE SWs is simulated in 80 μm long, 1.15 μm wide, and 10 nm thin stripes and, for comparison, in full films. The Gilbert damping parameter α_{sim} is either set to 0.0015 (i.e., to $\alpha_{\mathrm{int}}^{\mathrm{FMR}}$) or 0.0040 (i.e., to $\approx\alpha_{\mathrm{eff}}^{\mathrm{SW,exp}}$). All material parameters used correspond to the experimentally determined ones including the IP anisotropy. The images obtained from frequency sweeps at fixed H_0 and field sweeps at fixed f are analyzed in the same way as the Kerr images, and we obtain k, L_{att}, and v_{g} to deduce $\alpha_{\mathrm{eff}}^{\mathrm{SW,sim}}$ (see supplementary material).

In the following, we focus on the results for simulations without the IP anisotropy since it turns out that it does not cause significant changes in L_{att} (see supplementary material). For a perfect CoFe stripe, the characteristics of the SW dispersion in the f range of 13.68 to 14.16 GHz deduced from simulations at different bias fields are shown in Fig. 4(a). Figures 4(b) and 4(c) illustrate the corresponding field dependence of v_{g} and L_{att} at 13.92 GHz, respectively. Finally, based on these two quantities, the resulting $\alpha_{\mathrm{eff}}^{\mathrm{SW,sim}}$ values are depicted in Fig. 4(d). We find qualitative good agreement between simulation and experimental data for k and v_{g}. In the case of L_{att}, a good matching is achieved for $\alpha_{\mathrm{sim}} = 0.0040$. For $\alpha_{\mathrm{sim}} = 0.0015$, the L_{att} values extracted from the simulations are about 2.5 times larger than the experimental ones. As clearly visible in Fig. 4(d), within the error bars, the extracted $\alpha_{\mathrm{eff}}^{\mathrm{SW,sim}}$ value and the input damping parameter agree. These findings indicate that, in the poly-

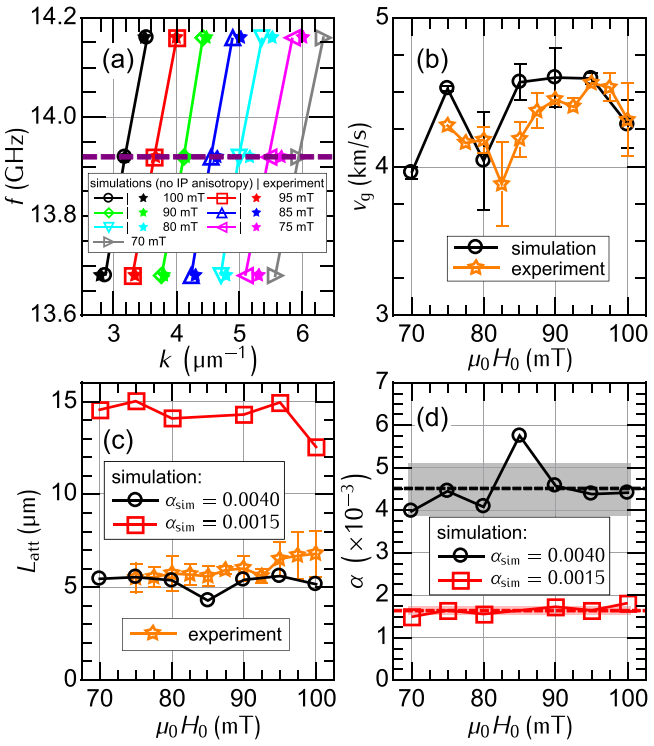

FIG. 4. Comparison of simulation and experimental results on the CoFe stripes. (a) SW dispersion at different bias fields [here, simulation without any IP anisotropy (open symbols) vs. experiment (stars)]. (b) Field dependence of v_g at 13.92 GHz [dashed line in (a)]. (c) Field dependence of L_{att} at 13.92 GHz for simulations performed using both $\alpha_{sim} = 0.0015 = \alpha_{int}^{FMR}$ and $\alpha_{sim} = 0.0040 = \alpha_{eff}^{SW,exp}$. (d) Comparison of the damping parameters deduced from the images obtained from simulations performed using either α_{sim} value. Dashed lines indicate the average values over the field range studied, while color-shaded areas denote the corresponding error range.

crystalline CoFe, the attenuation of propagating SWs is not solely determined by the intrinsic damping which is derived from the slope of $\Delta H(\omega)$ but is significantly enhanced by extrinsic contributions to the magnetic losses which manifest as a distinct inhomogeneous FMR linewidth broadening as clearly visible in Fig. 1(c). Both contributions seem to be able to be combined in an effective magnetic damping parameter. Indeed, according to the fit for the easy axis, $\mu_0 \Delta H(13.92\,\text{GHz}) = 3.49\,\text{mT}$. The slope of a straight line between the origin and that point corresponds to an effective magnetic damping of $\approx 3.8 \times 10^{-3}$, which is in good agreement with $\alpha_{eff}^{SW,exp}$. This approach reveals effective magnetic damping values ranging from ≈ 3.4 to 4.3×10^{-3} for $f = 10$–18 GHz. Consequentially, propagating SWs always suffer more attenuation than expected beforehand based solely on the low α_{int}^{FMR} value. This explanation is qualitatively supported by simulations performed with $\alpha_{sim} = \alpha_{int}^{FMR}$ and inhomogeneities added to the CoFe. The more pronounced the inhomogeneities are the shorter the attenuation length is and thus the larger the corresponding deduced $\alpha_{eff}^{SW,sim}$ value is.

In summary, the magnetic damping of 10 nm polycrystalline $Co_{25}Fe_{75}$ grown by MBE is experimentally investigated by both FMR on full films and SW propagation experiments in narrow stripes using TRMOKE. FMR reveals an intrinsic magnetic damping parameter of 1.5×10^{-3}. In contrast, the attenuation length of propagating DE SWs is only about 6 μm corresponding to a damping parameter of $\approx 4 \times 10^{-3}$. Based on the findings from micromagnetic simulations, this distinct difference is attributed to arise from the significant extrinsic contributions to the magnetic losses present in this poly-crystalline CoFe system, which cause a much stronger SW attenuation than expected solely based on the low intrinsic magnetic damping parameter. Overall, our findings prove that the binary 3*d* transition metal alloy CoFe can become a promising material for magnonic applications, when the extrinsic contributions to the damping can be further reduced. This can be achieved by optimizing the growth and by the choice and preparation of the substrate and the seed layer.

See supplementary material for additional measurement results, details about the implementation of the micromagnetic simulations using MuMax3 and details about the analysis of the experimental and simulation data.

We gratefully acknowledge funding by the Deutsche Forschungsgemeinschaft via SFB 689.

[1]V. V. Kruglyak, S. O. Demokritov, and D. Grundler, J. Phys. D: Appl. Phys. **43**, 260301 (2010).
[2]D. D. Stancil and A. Prabhakar, *Spin Waves - Theory and Applications* (Springer US, 2009).
[3]A. G. Gurevich and G. Melkov, *Magnetization Oscillations and Waves* (CRC Press, Boca Raton, 1996).
[4]Y. Sun, H. Chang, M. Kabatek, Y.-Y. Song, Z. Wang, M. Jantz, W. Schneider, M. Wu, E. Montoya, B. Kardasz, B. Heinrich, S. G. E. te Velthuis, H. Schultheiss, and A. Hoffmann, Phys. Rev. Lett. **111**, 106601 (2013).
[5]H. Yu, O. d'Allivy Kelly, V. Cros, R. Bernard, P. Bortolotti, A. Anane, F. Brandl, R. Huber, I. Stasinopoulos, and D. Grundler, Sci. Rep. **4**, 6848 (2014).
[6]A. Talalaevskij, M. Decker, J. Stigloher, A. Mitra, H. S. Körner, O. Cespedes, C. H. Back, and B. J. Hickey, Phys. Rev. B **95**, 064409 (2017).
[7]V. Vlaminck and M. Bailleul, Science **322**, 410 (2008).
[8]K. Sekiguchi, K. Yamada, S.-M. Seo, K.-J. Lee, D. Chiba, K. Kobayashi, and T. Ono, Phys. Rev. Lett. **108**, 017203 (2012).
[9]J.-Y. Chauleau, H. G. Bauer, H. S. Körner, J. Stigloher, M. Härtinger, G. Woltersdorf, and C. H. Back, Phys. Rev. B **89**, 020403(R) (2014).
[10]O. Gladii, D. Halley, Y. Henry, and M. Bailleul, e-print arXiv:1704.02217 [cond-mat.mtrl-sci].
[11]T. Sebastian, Y. Ohdaira, T. Kubota, P. Pirro, T. Brächer, K. Vogt, A. A. Serga, H. Naganuma, M. Oogane, Y. Ando, and B. Hillebrands, Appl. Phys. Lett. **100**, 112402 (2012).
[12]M. Zhu, B. D. Soe, R. D. McMichael, M. J. Carey, S. Maat, and J. R. Childress, Appl. Phys. Lett. **98**, 072510 (2011).
[13]H. Yu, R. Huber, T. Schwarze, F. Brandl, T. Rapp, P. Berberich, G. Duerr, and D. Grundler, Appl. Phys. Lett. **100**, 262412 (2012).
[14]S. Mankovsky, D. Ködderitzsch, G. Woltersdorf, and H. Ebert, Phys. Rev. B **87**, 014430 (2013).
[15]M. A. W. Schoen, D. Thonig, M. L. Schneider, T. J. Silva, H. T. Nembach, O. Eriksson, O. Karis, and J. M. Shaw, Nat. Phys. **12**, 839 (2016).
[16]R. W. Damon and J. R. Eshbach, J. Phys. Chem. Solids **19**, 308 (1961).
[17]R. D. McMichael, D. J. Twisselmann, and A. Kunz, Phys. Rev. Lett. **90**, 227601 (2003).
[18]G. Woltersdorf, F. Hoffmann, H. G. Bauer, and C. H. Back, Phys. Rev. B **87**, 054422 (2013).
[19]M. Haertinger, C. H. Back, J. Lotze, M. Weiler, S. Geprägs, H. Huebl, S. T. B. Goennenwein, and G. Woltersdorf, Phys. Rev. B **92**, 054437 (2015).
[20]M. A. W. Schoen, J. M. Shaw, H. T. Nembach, M. Weiler, and T. J. Silva, Phys. Rev. B **92**, 184417 (2015).
[21]M. Bailleul, D. Olligs, and C. Fermon, Appl. Phys. Lett. **83**, 972 (2003).
[22]A. Aharoni, J. Appl. Phys. **83**, 3432 (1998).
[23]Y. Henry, O. Gladii, and M. Bailleul, preprint arXiv:1611.06153 (2016).[cond-mat.mes-hall].
[24]A. Vansteenkiste, J. Leliaert, M. Dvornik, M. Helsen, F. Garcia-Sanchez, and B. Van Waeyenberge, AIP Adv. **4**, 107133 (2014).